THE ASTROPHYSICAL JOURNAL, 492:L95–L97, 1998 January 10

INITIAL ON-ORBIT PERFORMANCE OF NICMOS

RODGER I. THOMPSON, MARCIA RIEKE, GLENN SCHNEIDER, DEAN C. HINES, AND MICHAEL R. CORBIN
Steward Observatory, 933 North Cherry Avenue, University of Arizona, Tucson, AZ 85721-0065
Received 1997 July 23; accepted 1997 October 30; published 1997 December 30

ABSTRACT

On 1997 February 13, Space Shuttle astronauts placed the Near-Infrared Camera and Multiobject Spectrometer (NICMOS) into the *Hubble Space Telescope*. Following installation, the servicing mission orbital verification program (SMOV) performed extensive testing of the instrument to verify that it can be operated and calibrated effectively. This program is essentially completed, and routine science observations have begun in most of the NICMOS modes of operation. This Letter describes the performance levels of NICMOS at this time.

Subject headings: instrumentation: detectors — miscellaneous — space vehicles

1. INTRODUCTION

The Near-Infrared Camera and Multiobject Spectrometer (NICMOS) provides imaging, spectroscopic, polarimetric, and coronagraphic observations in the near-infrared (1.0–2.5 μm) with the *Hubble Space Telescope* (*HST*). Its primary purpose is to get diffraction-limited, high-resolution imaging throughout the spectral region and to exploit the lack of strong telluric OH^- emission at the *HST* orbital altitude. Experience with the NICMOS 3 infrared detectors developed for the mission indicated a response at wavelengths as short as 0.8 μm; therefore, filters were added to utilize this capability. This provides an overlap with the Wide Field Planetary Camera (WFPC) and Space Telescope and Imaging Spectrograph (STIS) wave bands for linking observations from the ultraviolet to the near-infrared. The thermal emission from the warm *HST* mirrors limits observations beyond 2.5 μm, and so the detectors were tuned to cut off at that wavelength. Details of the instrument and its operation are given by MacKenty et al. (1997).

2. IMAGING PERFORMANCE

We have excellent image performance data on the high-resolution cameras 1 and 2 from the servicing mission orbital verification (SMOV) activities. In-focus, image-quality data are not available for the WFPC3 since it is not currently within the range of the NICMOS focus adjustment mechanism. However, we do have a good characterization of the detector performance parameters, which are discussed in § 2.2. Table 1 gives the imaging characteristics of the three cameras. The difference between the *X* and *Y* pixel scales is due to the tilt of the image plane at the location of the detectors. This is primarily due to the off-axis placement of NICMOS. The difference was not considered significant enough to tilt the detectors in compensation for the field angle.

2.1. *Image Quality*

The observed image quality in cameras 1 and 2 match well with the expected image quality. Figure 1 compares the encircled energy as a function of radial distance for a point-spread function (PSF) computed using the software program TINY TIM (Krist 1995) and the encircled energy measured for a star image in camera 2. The filter was the broadband filter F160W, which has a center wavelength slightly shorter than the camera 2 diffraction limit wavelength of 1.75 μm. We define the diffraction limit as the wavelength where the camera has 5 pixels between the first zeros of the theoretical PSF for *HST*. Figure 1 shows that the actual encircled energy function is very close to the theoretical function. Figure 2 (Plate L5) compares the TINY TIM synthetic image with the camera 2 F160W filter image of an actual star observed with NICMOS. The only differences are attributable to the actual star image not being exactly centered on a pixel.

This special issue of the Astrophysical Journal Letters contains several plates and figures that demonstrate the image quality of the NICMOS cameras. As an example, note the plates in Stolovy et al. (1998), where the Airy rings of the diffraction pattern are well defined in the brighter stars in the plate. Also note the detection of several faint stars 3″–4″ away from a bright source nearly 10^4 times brighter in Thompson et al. (1998). This clearly shows the low scattering background in NICMOS and the advantages of detectors that do not leave trails of residual image near very bright objects because of charge transfer effects.

2.2. *Photometric Performance*

The photometric performance of NICMOS is close to the prelaunch estimates of the NICMOS instrument definition team. At this time, the Exposure Time Calculation tool maintained by the Space Telescope Science Institute (STScI) is undergoing a revision to reflect the true on-orbit performance of the instrument. Table 1 gives some of the basic photometric parameters for three cameras. These include the dark current, read noise, and gain. On-orbit measurements show that the background infrared flux levels are less than the levels expected before flight. This means that the cold baffling of the detectors is working well and that there are no unexpected thermal sources in the *HST* itself.

To date, none of the basic parameters such as noise, dark current, or gain have changed while in orbit. In a period of 3 months of monitoring in orbit, there has been no change in the dark current attributable to the action of cosmic rays on the detector. There also has been no change in the number of electrically bad pixels attributable to cosmic-ray damage.

The total photometric performance is a combination of all of the photometric parameters. SMOV activities included photometric tests in selected filters. The tests produced images of a standard star at three different locations on the array in four to five filters per camera. Table 2 gives the performance levels of the cameras in the measured filters along with the expected sensitivity for a 1000 s integration on a point source. The sensitivity number is expressed as the flux of a point source in units of janskys that will give a signal-to-noise (S/N) ratio

TABLE 1
NICMOS Camera Parameters

Camera	*X* Pixel[a]	*Y* Pixel[a]	*X* FOV[b]	*Y* FOV[b]	P.A. V3[c]	DC[d]	RN[e]	Gain[f]
1	0.043328	0.043131	11.09197	11.04154	315.33	0.16	22.0	5.4
2	0.076261	0.075502	19.52282	19.32851	314.52	0.15	29.0	5.4
3	0.204538	0.203916	52.36173	52.20250	314.86	0.15	30.0	6.5

[a] The pixel size is in units of arcseconds, measured on 1997 May 15.
[b] The field of view is in units of arcseconds, measured 0n 1997 May 15.
[c] P.A. V3 is the position angle of the image *y*-axis relative to the +V3 axis of the *HST*.
[d] The dark current is in units of electrons per second.
[e] The read noise is in units of electrons for a 2048 s MULTIACCUM sequence.
[f] In units of electrons per ADU.

of 1 in a full aperture of six Airy rings photometric reduction. Measured background levels are not given for camera 3 since, in its current out-of-focus state, it has significant vignetting that produces a high thermal background. We expect to eliminate the vignetting in actual operation through a motion of the Field Offset Mirror.

2.2.1. *Photometric Features*

Investigators processing NICMOS images should be aware of two features that, if not compensated for, could compromise the quality of the final results. The first is a residual charge present in images taken after NICMOS has been in the "auto-flush" mode. Any time a detector is idle, it reverts to this mode; therefore, the first reads of any sequence of observations are subject to this effect. The residual charge is on the order of 30–40 analog-to-digital converter units (ADUs) (~200 electrons) per pixel. The second image has about half this signal, and subsequent images have little or no residual. In this context, an image means a full MULTIACCUM or ACCUM sequence, not the individual reads in a sequence. The proper way to address this feature is to subtract the first dark in a dark sequence from the first image in an image sequence, the second dark from the second image, and then the median of the remaining darks in a sequence from the remaining images. If a sequence has spatial dithering, NICMOS goes into the auto-flush mode while the telescope is moving. If the move is on the order of an arcsecond or less, the residual is partially restored, and usually an average of the first and second darks is the proper dark to subtract from the remaining dithered images. This must be done by the observer since the STScI pipeline does not know the sequence of images and darks. Column 127 (first column is 0) is particularly sensitive to this, and images that do not properly compensate for the effect can have a cosmetically annoying stripe along the column. This has been termed the "pedestal effect" by STScI.

A second effect is only present in images that have been heavily saturated in the first one or two reads of a MULTIACCUM sequence. The NICMOS arrays are divided into quadrants that are read out simultaneously. When the readout encounters a heavily saturated area, there is a slight change in readout level in all rows. This produces an electrical offset that appears as a stripe in the columns that are saturated and in their counterparts in the other quadrants. The plate in Thompson et al. (1998) shows this effect. Most observations will not encounter this effect since it requires a high degree of saturation in the first few reads to be noticeable.

3. SPECTROSCOPIC PERFORMANCE

Three grisms located in the camera 3 filter wheel provide multiobject spectroscopy at all wavelengths. Since camera 3 is not yet in focus, we have only verified that the registration of the spectral image relative to the undispersed object image is the same as observed in thermal vacuum testing previous to flight. Background levels in each of the grisms are consistent with the equivalent filters.

4. POLARIZATION PERFORMANCE

The NICMOS cameras 1 and 2 each contain a set of three Polarcore polarizers on a wide-band filter. The polarization angles are set roughly 120° apart with bandpasses of 0.81–1.29 and 1.9–2.1 μm for cameras 1 and 2, respectively. Preflight thermal vacuum testing indicated that the polarizers did not

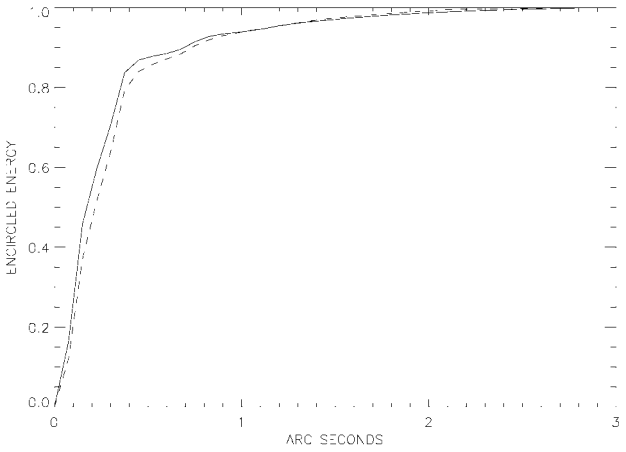

Fig. 1.—Comparison of the encircled energy vs. the radial distance for a computed PSF (*solid line*) and for an observed PSF (*dashed line*).

TABLE 2
NICMOS Photometric Performance

Camera	Filter	e (s^{-1} Jy^{-1})	Background[a]	Flux for S/N = 1[b]
1	F090M	3.72×10^5	0.10	1.83×10^{-7}
1	F110M	7.10×10^5	0.11	9.51×10^{-8}
1	F145M	9.25×10^5	0.13	7.00×10^{-8}
1	F165M	1.12×10^6	0.20	5.93×10^{-8}
2	F110W	2.37×10^6	0.30	3.62×10^{-8}
2	F165M	1.16×10^6	0.26	7.39×10^{-8}
2	F207M	8.49×10^5	0.59	2.29×10^{-7}
2	F222M	8.93×10^5	9.00	3.91×10^{-7}
2	F237M	1.12×10^6	39.0	6.26×10^{-7}
3	F110W	2.12×10^6	...	3.33×10^{-8}
3	F160M	2.17×10^6	...	3.64×10^{-8}
3	F166N	9.76×10^4	...	5.45×10^{-7}
3	F222M	9.00×10^5	...	7.76×10^{-7}
3	F240M	1.47×10^6	...	1.41×10^{-6}

[a] Flux in units of electrons per second per pixel.
[b] Flux in units of janskys of a point source with 1000 s integration.

have equal efficiencies and that the position angles between each polarizer differed slightly from the nominal 120°. For each polarizer, the efficiency across the field of view is constant, and the instrumental polarization for both cameras is ≈1%, indicating very excellent optical coatings. Table 3 lists the results.

The unequal efficiencies and nonideal position angle offsets require a modification of the simple reduction procedure outlined in the NICMOS manual. This modified procedure was successfully tested on camera 2 observations of the highly polarized Egg Nebula obtained during the Early Release Observations (Sahai et al. 1998), which reveal a wealth of structure not previously seen. This reference also contains a description of the modified method. In areas of the Egg Nebula where the structure appears fairly uniform, the variation in the polarization implies $\sigma_p \approx \pm 5\%$. Based on our current understanding of the system, observations using the polarizers in cameras 1 and 2 of NICMOS are capable of providing high spatial resolution polarization information for bright and highly polarized objects with uncertainties $\sigma_p \approx 5\%$.

TABLE 3

CHARACTERISTICS OF NICMOS POLARIZERS

Filter	Polarizer Efficiency[a]	Δ (P.A.)[b]
POL0S	0.972	...
POL120S	0.477	114.88
POL240S	0.768	142.42
POL0L	0.731	...
POL120L	0.629	122.58
POL240L	0.874	116.76

[a] Maximum = 1.

[b] The position angle between the principle axes of the polarizers.

5. CORONAGRAPHIC PERFORMANCE

Camera 2 has a coronagraphic capability that is comprised of two optical elements. The camera 2 field divider mirror contains a 160 μm diameter hole that covers 93% of the encircled energy of a stellar PSF at 1.6 μm. The hole lowers both the diffracted energy in the surrounding region and the downstream scattering. The radius of the occulting spot is 4 pixels (or 0.″3) at the detector focal plane. The spot appears at an approximate location of (−3.″5, +5.″5) from the (+*Y*, −*X*) corner in all camera 2 images. The second element is a cold pupil-plane mask at ~100 K that masks the primary mirror edge, the secondary, the hole, the secondary spider, and the hold-down pads in order to further reduce the diffracted energy. The primary purpose of this mask, however, is the suppression of thermal emission from the telescope structures.

SMOV demonstrated that targets as bright as $H = 3.8$ may be autonomously positioned in the center of the hole to better than $\frac{1}{4}$ of a pixel. Near the edge of the hole, preliminary performance figures at 1.6 μm indicate that the diffracted and scattered energy background reduction is a factor of ~8 and declines to a factor of ~3 at radial distances between 0.″6 and 1.″3. This factor declines to an average of ~2.4 out to a radius of ~3″. The best performance levels occur with the stellar focus on the coronagraphic hole rather than on the detector, which causes a small focus error at the detector. The focus wave-front error at 1.6 μm is less than λ/12, which reduces the ensquared energy in the 9 central pixels by only 3.3% compared with imaging at optimal focus. Further tests are under way to optimize the coronagraphic performance.

6. INSTRUMENT LIFETIME AND CAMERA 3 FOCUS

As of the time of the submission of this Letter, 1997 July 31, camera 3 is continuing to return toward the range of focus of the NICMOS instrument. The return is due to cryogen loss in the area that has pushed the focus forward when the cryogen warmed from its preflight cold hold values. The rate of return has been variable, as should be expected from the complicated Dewar geometry. The average current rate of return indicates that the camera may come within focus range in the late fall of this year. The large number of parameters from metallurgy to stress analysis makes this prediction very tentative.

The same forward motion of the Dewar cold well that produced the focus problem also produced a thermal contact between the nitrogen cold well and the vapor-cooled shield surrounding the nitrogen tank. The resultant increase in thermal conductivity has increased the net heat load on the solid nitrogen cryogen. If the thermal contact persists throughout the lifetime of the instrument, the current projected lifetime terminates at the end of 1999 January. Since the thermal contact initiated at the same time as the camera moved out of focus range, the contact may release when and if the camera returns to focus. Under these conditions, the eventual lifetime will depend on the time of the termination of the thermal contact.

The NICMOS team wishes to thank the dedicated personnel at Ball Aerospace, Rockwell International, NASA Goddard Space Flight Center, NASA Headquarters, and the Space Telescope Science Institute, who have worked over the last 13 years to make this mission possible. We also greatly thank the crew of STS 82, who installed NICMOS into *HST* along with STIS and greatly improved the overall performance of the telescope. NICMOS was built under NASA contract NASA 5-31289, and this work is supported in part by NASA grant NAG 5-3042. This Letter is based on observations with the NASA/ESA *Hubble Space Telescope*, obtained at the Space Telescope Science Institute, which is operated by the Association of Universities for Research in Astronomy, Inc., under NASA contract NAS5-26555.

REFERENCES

Krist, H. 1995, in ASP Conf. Ser. 77, Astronomical Data Analysis Software and Systems, IV, ed. R. A. Shaw, H. E. Payne, & J. J. E. Hayes (San Francisco: ASP), 349

MacKenty, J. W., Skinner, C., Calzetti, D., & Axon, D. 1997, NICMOS Instrument Handbook, Version 2.0 (Baltimore: STScI)

Sahai, R., Hines, D. C., Kastner, J. H., Weintraub, D. A., Trauger, J. T., Rieke, M. J., Thompson, R. I., & Schneider, G. 1998, ApJ, 492, L163

Stolovy, S. R., et al. 1998, ApJ, 492, L151

Thompson, R. I., Corbin, M., Young, E., & Schneider, G. 1998, ApJ, 492, L177

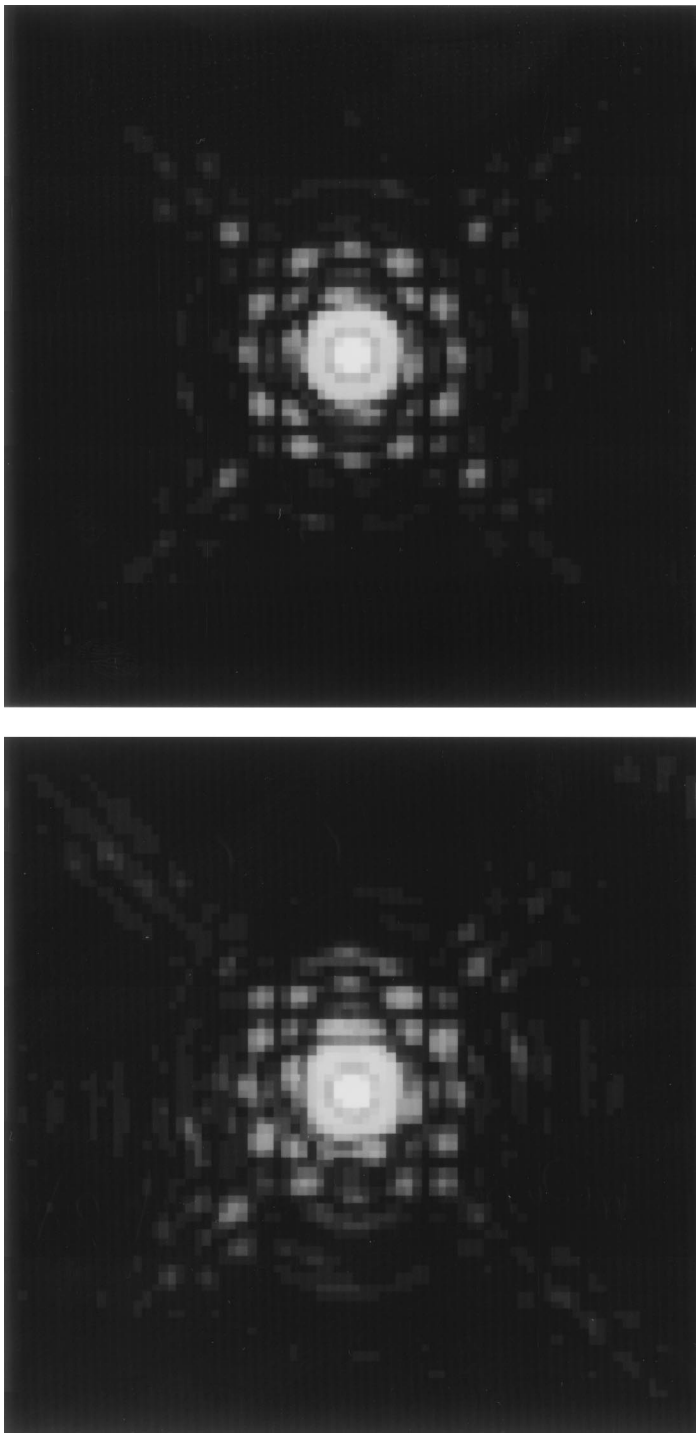

FIG. 2.—Comparison of the TINY TIM–generated PSF image (*top*) and an actual image in the camera 2 F160W filter (*bottom*)

THOMPSON et al. (see 492, L95)